Journal of Solid State Chemistry 184 (2011) 1813–1819

Contents lists available at ScienceDirect

Journal of Solid State Chemistry

journal homepage: www.elsevier.com/locate/jssc

Synthesis, structure and electrical properties of $Cu_{3.21}Ti_{1.16}Nb_{2.63}O_{12}$ and the CuO_x–TiO_2–Nb_2O_5 pseudoternary phase diagram

Nik Reeves-McLaren*, Matthew C. Ferrarelli, Yuan-Wei Tung, Derek C. Sinclair, Anthony R. West

Department of Materials Science and Engineering, University of Sheffield, Sheffield, S1 3JD, UK

ARTICLE INFO

Article history:
Received 28 December 2010
Received in revised form
20 May 2011
Accepted 23 May 2011
Available online 30 May 2011

Keywords:
$Cu_{3.21}Ti_{1.16}Nb_{2.63}O_{12}$
CCTO
Perovskite
Rutile
Rietveld
Impedance

ABSTRACT

Subsolidus phase relations in the CuO_x–TiO_2–Nb_2O_5 system were determined at 935 °C. The phase diagram contains one new phase, $Cu_{3.21}Ti_{1.16}Nb_{2.63}O_{12}$ (CTNO) and one rutile-structured solid solution series, $Ti_{1-3x}Cu_xNb_{2x}O_2$: $0 < x < 0.2335$ (35). The crystal structure of CTNO is similar to that of $CaCu_3Ti_4O_{12}$ (CCTO) with square planar Cu^{2+} but with *A* site vacancies and a disordered mixture of Cu^+, Ti^{4+} and Nb^{5+} on the octahedral sites. It is a modest semiconductor with relative permittivity ~63 and displays non-Arrhenius conductivity behavior that is essentially temperature-independent at the lowest temperatures.

1. Introduction

The $A'A''_3B_4O_{12}$: A'=Ca, Cd, Na, Y, Ln, A''=Cu, Mn, B=Ti, Mn, family of perovskite-like phases has been extensively studied due to the presence of interesting structural and physical properties among the different family members [1–4]. The $A'A''_3B_4O_{12}$ structure, space group $Im\bar{3}$, is a distorted variant of the simple cubic ABO_3 perovskite structure, space group $Pm\bar{3}m$. The 1:3 ordering of the large A' and small A'' cations results in a $2\times2\times2$ supercell with $a=2a_{perovskite}\simeq 7.4$ Å. The structure has heavily rotated BO_6 octahedra, $a^+a^+a^+$ in Glaser notation [5]; the structure retains cubic symmetry and the coordination sphere of the A' site remains 12 fold [6]. The A'' site coordination sphere, however, becomes square planar or slightly rectangular, depending on the angle of rotation of the BO_6 octahedra.

An extensive range of cations can be accommodated on the A' and B sites but with the A'' site restricted to cations, which have a preference for square-planar coordination, *e.g.*, Cu^{2+} and Mn^{3+}. Depending on the combination of cation valences, charge balance can also be achieved by vacancies on any of the cation sites. A wide variety of physical properties are exhibited by this structure-type, including antiferromagnetism, ferromagnetism, ferrimagnetism, magnetoresistance and high extrinsic permittivity [4,7–11].

Since 2000, the $ACu_3Ti_4O_{12}$ subgroup has been extensively investigated because of high extrinsic permittivity, ε', observed in these materials at room temperature (RT) [10,11]. For $CaCu_3Ti_4O_{12}$ (CCTO), the most studied member of the subgroup, the cause of the high extrinsic permittivity is generally accepted to be a combination of the material itself being semiconducting at RT ($\sigma_{RT}\sim$5–100 mS cm^{-1}) and an electrically inhomogeneous microstructure in the case of ceramics or non-ohmic sample-electrode contacts in the case of single crystals [1,2,12]. The microstructure of CCTO ceramics consists of n-type semiconducting grains surrounded by thin insulating regions at the grain boundaries. The origin of the semiconductivity in CCTO and related phases is still unresolved but has been linked to mixed Ti^{3+}/Ti^{4+} on the *B*-site. The magnitude of the conductivity is dependent on processing conditions, with higher sintering temperatures and/or longer sintering periods producing higher RT bulk conductivity [13]. The origin of the conductivity may therefore be associated with oxygen or CuO_x-loss and/or cation non-stoichiometry, and involve Cu^+/Cu^{2+} on the A'' site as well as Ti^{3+}/Ti^{4+} on the *B* site.

An initial investigation into Nb-doping of CCTO ceramics, the results of which will be published elsewhere, found a Ca-free composition that was almost single phase, and whose XRD data appeared similar to that of CCTO. The purpose of this current study is to investigate the phase relations in the CuO_x–TiO_2–Nb_2O_5 system, with particular reference to this previously unreported phase with an *A*-site deficient CCTO-like structure.

2. Experimental

The reagents used were CuO (99%), Nb_2O_5 (99.9%) and TiO_2 (99.9%), all from Sigma-Aldrich, dried at 700 °C. Appropriate

* Corresponding author. Fax: +44 1142225943.
E-mail address: n.reeves@sheffield.ac.uk (N. Reeves-McLaren).

0022-4596/$ - see front matter © 2011 Elsevier Inc. All rights reserved.
doi:10.1016/j.jssc.2011.05.032

amounts of each reagent were mixed in an agate mortar and pestle, then fired in Pt foil boats at 935 °C for 60 h with intermittent regrinding.

X-ray Powder Diffraction (XRD) used a STOE STADI P diffractometer, Cu $K\alpha_1$ radiation ($\lambda = 1.54056$ Å) using either an imaging plate detector, for phase analysis, or a linear position sensitive detector, for lattice parameter or structural refinement. Initial data analysis used STOE's WinX^{POW} software package. Rietveld refinement used the EXPGUI [14] interface for GSAS [15]; the errors quoted are as given by GSAS. Initial isotropic thermal parameters, U_{iso}s, were 0.025 Å^2 for all positions. Several constraints were applied at the start of refinement. The thermal parameters were constrained to be the same for all atoms sharing a particular site. The total occupancy of sites was set to unity. The background and scale factors were refined first, using a shifted Chebyschev function with 6 terms for the background, followed by the lattice and profile parameters. Atomic positions were refined in order of scattering power; where the refinement indicated that a site was shared by multiple cations, atomic coordinates, thermal parameters or fractions were refined simultaneously as appropriate. The whole process was repeated to convergence with negligible shifts in atomic variables.

Pellets were pressed from powders uniaxially to 40 MPa in an 8 mm die, and then pressed isostatically to 200 MPa using a cold isostatic press (Model: 32330, Flow Autoclave Systems Inc.). Pellets were fired at 935 °C for 2 h with a heating and cooling rate of 5 °C/min.

For impedance spectroscopy (IS) measurements, pellets were polished with SiC grinding paper and then coated on opposite parallel plane faces with sputtered Au. Low temperature IS data, 10–300 K, were collected over the frequency range 25 Hz–1 MHz using a precision LCR meter (Model: E4980A, Agilent Technologies Inc.) with an applied ac voltage of 100 mV. A cryostat (Model: CCC1104, Oxford Instruments plc), cold head (Model: 2/9, Edwards) and closed cycle He compressor (Model: Cryodrive 1.5, Edwards) controlled by a temperature controller (Model: ITC503S, Oxford Instruments) were used to cool the sample in vacuum. All IS data were corrected for sample geometry, any stray resistance, inductance and capacitance inherent in the measuring setup and analyzed using the ZView software package [16].

3. Results and discussion

3.1. Doped rutile solid solutions, $Ti_{1-3x}Cu_xNb_{2x}O_2$

There have been numerous reports, where TiO_2 has been successfully doped with limited amounts of other metal cations. Rutile solid solutions including up to ca. 10–15 mol% Nb_2O_5 have been reported, with the maximum extent quoted at 1445–1475 °C in the literature [17].

With this in mind, attempts were made to synthesize compositions with TiO_2 co-doped with Cu and Nb according to the general formula $Ti_{1-3x}Cu_xNb_{2x}O_2$ and substitution mechanism:

$$3Ti^{4+} \rightarrow 2Nb^{5+} + Cu^{2+}$$

Compositions in the range $0 < x \leq 0.33$ were synthesized at 935 °C as described above, removed from the furnace and allowed to cool in air.

Compositions with $x = 0.01$–0.23 yielded phase-pure samples, which were indexed using the rutile space group, $P4_2/mnm$, showing that co-doping of TiO_2 with Cu and Nb according to the mechanism above occurred. Compositions with $x \geq 0.237$ gave a three-phase mixture of the rutile solid solution and both the orthorhombic and monoclinic polymorphs of $CuNb_2O_6$ [18], showing the limit for this previously-unreported solid solution to be 0.2335 ± 0.0035 at 935 °C.

Lattice parameters of the rutile solid solutions versus composition are presented in Fig. 1; although the variation of cell volume with composition is essentially linear, obeying Vegard's Law, a and c show small and opposite departures from linearity. The cell parameters and volume increase with Cu/Nb content, which can be rationalized in terms of the relative ionic radii [19] for Ti^{4+} (0.605 Å), Cu^{2+} (0.73 Å) and Nb^{5+} (0.64 Å) in octahedral coordination.

In order to investigate the possibility of (i) a range of anatase solid solutions existing at low temperatures, particularly in Ti-rich compositions, and (ii) variation with temperature in the maximum extent of the rutile solid solutions in Cu/Nb-rich specimens, small portions of selected compositions were annealed at various temperatures.

No anatase phase was observed for any composition annealed over the range 400–1000 °C. Since analysis of XRD data collected for compositions with $x = 0.01$ and 0.02 showed the presence of only a single rutile phase, it is likely that either the maximum extent of any anatase solid solution, if it does occur, is extremely

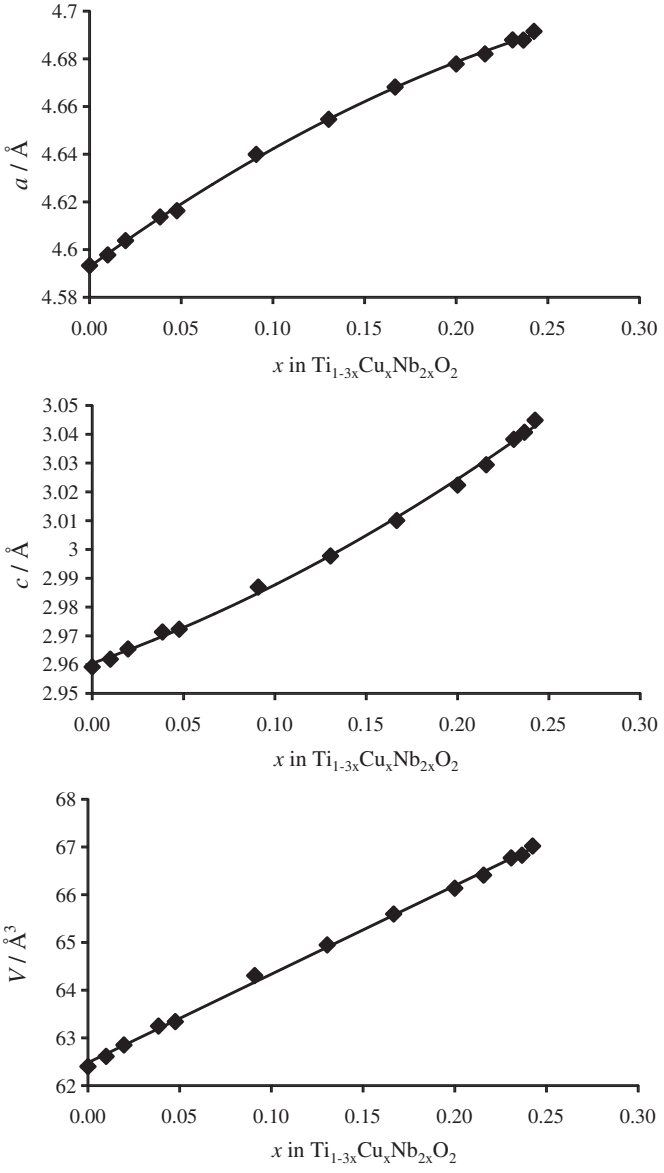

Fig. 1. Refined lattice parameters for rutile solid solutions, $Ti_{1-3x}Cu_xNb_{2x}O_2$. Error bars are smaller than the data points.

limited, or that the activation barrier for conversion of the rutile phase, once formed, to anatase is very high.

XRD patterns for $x=0.242$, 0.25 and 0.286, annealed at various temperatures (400–1000 °C) for 15 h, showed a significant increase in the intensity of Bragg peaks corresponding to the secondary phase, $CuNb_2O_6$, with decreasing annealing temperature. Samples of $x=0.216$ showed a single rutile phase down to 600 °C, but the appearance of a small amount of $CuNb_2O_6$ after annealing at 400 °C. Furthermore, samples of $x=0.242$ and 0.25 became single phase when annealed at 1000 °C. These data indicate that the maximum extent of solid solution increases with temperature and confirm Norwig et al.'s report [20] on the formation of a $Cu_{0.5}Ti_{0.5}NbO_4$ (*i.e.* $x=0.25$) phase. The TiO_2–$CuNb_2O_6$ binary phase diagram over the temperature range 400–1000 °C constructed using these data is shown in Fig. 2.

In order to verify the crystal structure of this proposed rutile solid solution, Rietveld refinement of RT XRD data was carried out for one composition, $x=0.2$. The data were fully indexed using the $P4_2/mnm$ space group, $a=4.67791$ (3) Å, $c=3.02234$ (2) Å and $V=66.137$ (1) Å^3. The structural model used, Table 1, had Ti, Cu and Nb sharing the 2*a* site, with oxygen fully occupying the 4*f* site. The statistical measures observed were good, with $\chi^2=6.58$ and discrepancy values of $R_{wp}=7.27\%$ and $R_p=5.58\%$. The visual fit of the data, Fig. 3, was extremely good. The calculated bond lengths, Table 1, were reasonable.

3.2. Structure refinement of $Cu_{3.21}Ti_{1.16}Nb_{2.63}O_{12}$

During study of the CuO–Nb_2O_5–TiO_2 system a new, previously-unreported phase was discovered and isolated phase-pure when reacting 56.464 mol% CuO, 20.404 mol% TiO_2 and 23.131 mol% Nb_2O_5. This composition (CTNO) lies on a join between the hypothetical compounds $Cu_3Ti_2Nb_2O_{12}$ and $Cu_{3.5}Nb_{3.5}O_{12}$, *i.e.,* at $x=0.21$ in $Cu_3^{2+}[Ti_{2-4x}^{4+}Nb_{2+3x}^{5+}Cu_x^{+}]O_{12}$. Compositions prepared with slightly different cation ratios were uniformly found to contain secondary phases, suggesting that this new compound exists as a non-stoichiometric line phase.

All reflections were indexed on a cubic unit cell, $a=7.47946$ (4) Å, space group $Im\bar{3}$. From its XRD pattern, which was similar to that of CCTO, it seemed that this new phase may be structurally related to CCTO.

Rietveld refinement of RT XRD data was carried out, using the structure of $A'A''_3B_4O_{12}$-type CCTO as the initial structural model: since this new compound was Ca-free, the 12-coordinate A' site was left empty; the A'' site (6*b* in the Wyckoff notation) was fully occupied by Cu^{2+}; Ti, Cu and Nb shared the octahedral B (8*c*) site; oxygen fully occupied the 24*g* site.

After simultaneous refinement of all appropriate parameters, the visual fit of the data, Fig. 4, was extremely good as were the various quality indicators: $\chi^2=1.365$, $R_{wp}=9.41\%$ and $R_p=7.13\%$. Isotropic thermal parameters, U_{iso}s, for the three sites were all acceptable. Final refined structural parameters are given in Table 2. Refinements of alternative crystal structures, *e.g.*, with the Cu^+ moved onto the A' site and a partially occupied B site led to poorer statistical measures, and had a deleterious effect on the quality of the visual fit.

Table 1
Structure refinement parameters and bond lengths for $Ti_{0.4}Cu_{0.2}Nb_{0.4}O_2$ at RT.

Space group	$P4_2/mnm$
a (Å)	4.67791 (3)
c (Å)	3.02234 (2)
V (Å^3)	66.137 (1)
χ^2	6.575
R_{wp} (%)	7.27
R_p (%)	5.58
Cation site	2*a*
$x(=y=z)$	0.0
Site occupancy	0.4 Ti/0.2 Cu/0.4 Nb
U_{iso} (Å^2)	0.0080 (3)
Oxygen site	4*f*
$x(=y)$	0.30345 (32)
z	0.0
Site occupancy	1.0 O
U_{iso} (Å^2)	0.0119 (7)
Bond lengths	
[Cation]—O (Å)	1.9936 (14) × 4
	2.0075 (21) × 2

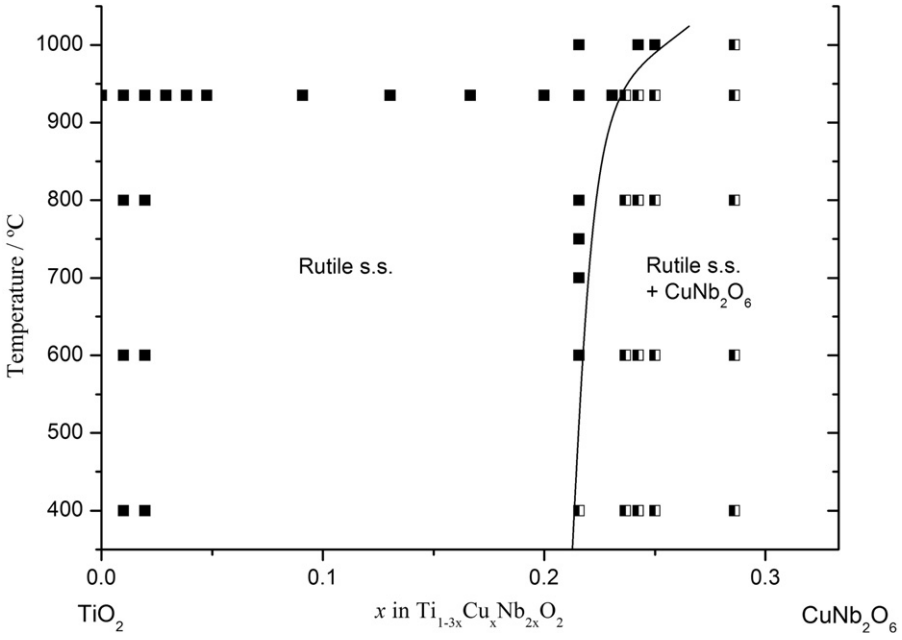

Fig. 2. Phase diagram for the TiO_2–$CuNb_2O_6$ join at temperatures below 1000 °C. Closed (■) and half closed (◧) refer, respectively, to 1-, 2-phase products. (No distinction is made between the different polymorphs of $CuNb_2O_6$).

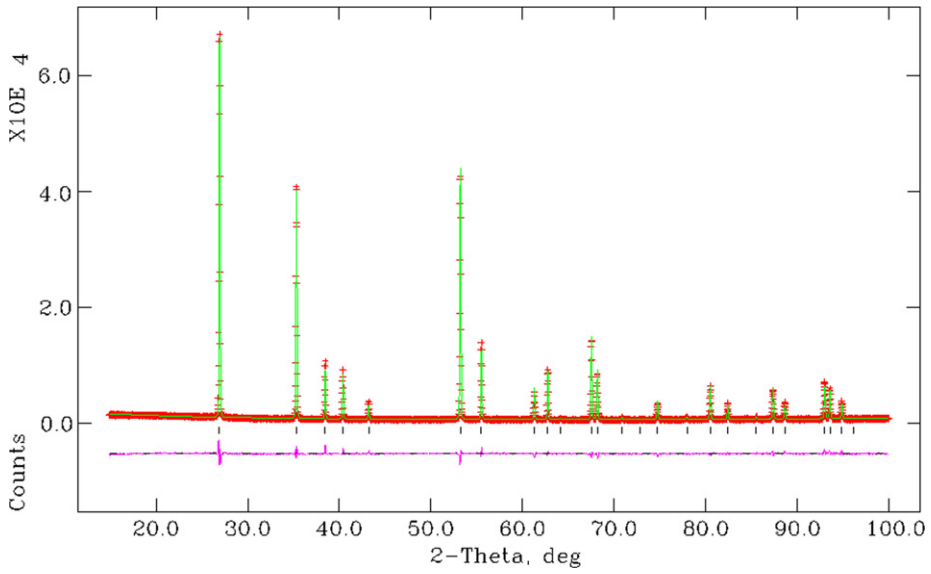

Fig. 3. Observed, calculated and difference profiles from XRD data of $Ti_{0.4}Cu_{0.2}Nb_{0.4}O_2$ at RT.

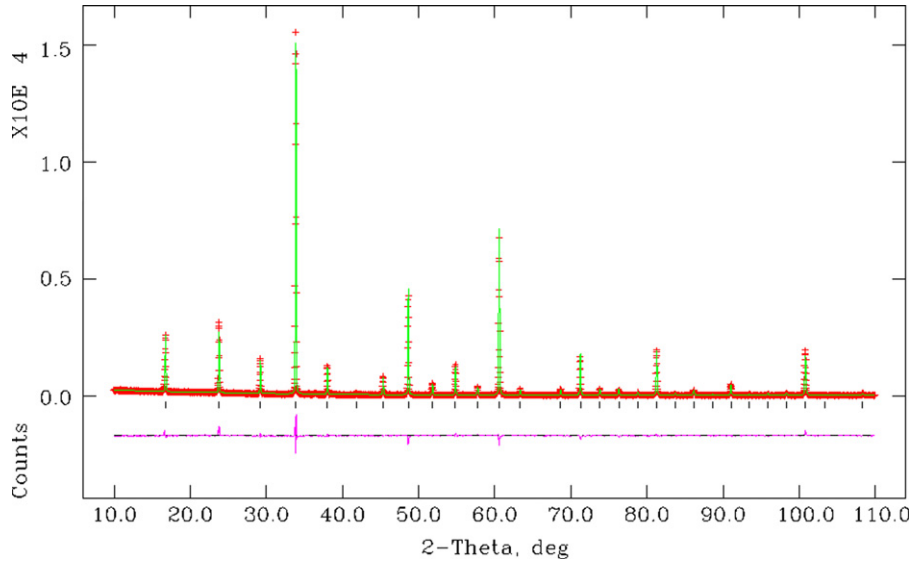

Fig. 4. Observed, calculated and difference profiles from XRD data for $Cu_{3.21}Ti_{1.16}Nb_{2.63}O_{12}$ at RT.

The crystal structure of CTNO, Fig. 5, can be described as a network of corner-sharing tilted BO_6 octahedra, with most of the Cu ions located in interstitial square planar A'' sites. The A''–O bond length of 2.0111 (28) Å is reasonable for square planar Cu^{2+}–O; the B–O bond length of 1.9744 (9) Å is a little shorter than expected, considering the relative ionic radii [19] for Ti^{4+} (0.605 Å), Cu^{+} (0.77 Å) and Nb^{5+} (0.64 Å) in octahedral coordination. However, the reported Ti–O bond length in CCTO is also shorter (quoted variously [21,22] as 1.95–1.96 Å) than might be anticipated from the relative ionic radii for Ti^{4+} in octahedral coordination.

The B–O–B bond angle of 142.54 (16)° indicates a severe rotation of the BO_6 octahedra. This rotation represents a major distortion of the ideal cubic perovskite structure, where all B–O–B angles are 180°, and is similar to that in CCTO, where the B–O–B angles are ca. 141°. Variants of the $A'A''_3B_4O_{12}$ structure with the A' site either partially (*e.g.*, $Ce_{1/2}\square_{1/2}Cu_3Ti_4O_{12}$, $RE_{2/3}\square_{1/3}Cu_3Ti_4O_{12}$) or completely vacant (*e.g.*, $\square Cu_3Ti_2Ta_2O_{12}$, $\square Cu_3Ti_2Sb_2O_{12}$, $\square Cu_2\square Ta_4O_{12}$) have previously been reported [21], but this is the first report of such a phase in the CuO–Nb_2O_5–TiO_2 ternary system.

It is assumed, but not proven, that $Cu_{3.21}Ti_{1.16}Nb_{2.63}O_{12}$ has mixed Cu valence and can be represented more fully as $Cu^{2+}_3(Cu^{+}_{0.21}Ti^{4+}_{1.16}Nb^{5+}_{2.63})O_{12}$ in which square planar A'' sites are fully occupied by Cu^{2+} and octahedral B sites are fully occupied by a disordered mixture of Cu^{+}, Ti^{4+} and Nb^{5+}. Further studies are underway to confirm this proposed stoichiometry.

3.3. The CuO_x–TiO_2–Nb_2O_5 pseudoternary phase diagram

The subsolidus phase relations in the CuO_x–TiO_2–Nb_2O_5 system have not been reported previously; they were determined here following heat treatments on 43 compositions, Table 3. Samples were reacted at 935 °C for 60 h; samples heated at lower temperatures or for less time often failed to react fully. The phase diagram, Fig. 6, consists of one new ternary phase, $Cu_{3.21}Ti_{1.16}Nb_{2.63}O_{12}$, and one solid solution series, $Ti_{1-3x}Cu_xNb_{2x}O_2$: $0 < x < 0.2335 \pm 0.0035$ at 935 °C. Since the phase $Cu_{3.21}Ti_{1.16}Nb_{2.63}O_{12}$ contains a mixture of Cu^{+} and Cu^{2+}, the phase diagram is not truly ternary but represents a section through the quaternary system CuO–Cu_2O–TiO_2–Nb_2O_5. For this reason,

Table 2
Structure refinement parameters and bond lengths for $Cu_{3.21}Ti_{1.16}Nb_{2.63}O_{12}$ at RT.

Space group	$Im\overline{3}$
a (Å)	7.47946 (4)
V (Å)	418.418 (7)
χ^2	1.365
R_{wp} (%)	9.41
R_p (%)	7.13
Cation site, A''	6*b*
x	0.0
y $(=z)$	0.5
Site occupancy	1.0 Cu
U_{iso} (Å^2)	0.0234 (4)
Cation site, B	8*c*
$x(=y=z)$	0.25
Site occupancy	0.29 Ti/0.052 Cu/0.658 Nb
U_{iso} (Å^2)	0.0205 (3)
Oxygen site	24*g*
x	0.0
y	0.30729 (34)
z	0.18752 (38)
Site occupancy	1.0 O
U_{iso} (Å^2)	0.0177 (10)
Bond lengths	
A''–O (Å)	2.0111 (28) × 4
B–O (Å)	1.9744 (9) × 6
Bond angles	
O–A''–O (deg)	88.45 (15)
	91.56 (15)
	180.0
O–B–O (deg)	88.12 (10)
	91.88 (10)
	180.0
B–O–B (deg)	142.54 (16)

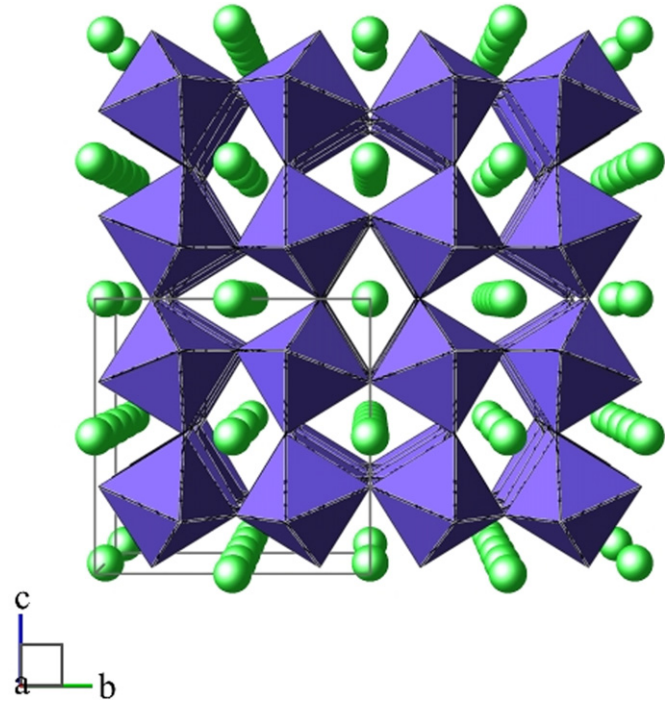

Fig. 5. Crystal structure of $Cu_{3.21}Ti_{1.16}Nb_{2.63}O_{12}$. Cu ions on the A″ site are shown as green spheres, with BO_6 octahedra in blue. (For interpretation of the references to color in this figure legend, the reader is referred to the web version of this article.)

Table 3
Phases present in different compositions after reaction at 935 °C.

Code	% CuO	% Nb_2O_5	% TiO_2	Phases present[a]
1	52.94	19.61	27.45	$Cu_{3.21}Ti_{1.16}Nb_{2.63}O_{12}$+C+R
2	56.52	21.74	21.74	$Cu_{3.21}Ti_{1.16}Nb_{2.63}O_{12}$+C
3	33.33	33.33	33.33	R+CN
4	52.50	23.75	23.75	$Cu_{3.21}Ti_{1.16}Nb_{2.63}O_{12}$+R
5	30.00	50.00	20.00	T_2N_5+CN+R
6	10.00	50.00	40.00	R+T_2N_5
7	40.00	40.00	20.00	CN+R
8	10.00	30.00	60.00	T_2N_5+R
9	25.00	25.00	50.00	R
10	20.00	20.00	60.00	R
11	15.00	15.00	70.00	R
12	10.00	10.00	80.00	R
13	5.00	5.00	90.00	R
14	30.00	30.00	40.00	R
15	0.00	71.43	28.57	T_2N_5
16	0.00	14.00	96.00	R+TN
17	8.00	80.00	12.00	T_2N_5+CN+N
18	1.00	49.00	50.00	T_2N_5+TN+R
19	2.00	48.00	50.00	T_2N_5+R
20	1.00	13.00	86.00	TN+R
21	4.00	10.00	86.00	TN+R
22	1.00	1.00	98.00	R
23	2.00	2.00	96.00	R
24	3.00	3.00	94.00	R
25	4.00	4.00	92.00	R
26	42.00	32.00	26.00	$Cu_{3.21}Ti_{1.16}Nb_{2.63}O_{12}$+CN+R
27	58.00	32.00	10.00	$Cu_{3.21}Ti_{1.16}Nb_{2.63}O_{12}$+CN+$C_3N$
28	72.00	18.00	10.00	$Cu_{3.21}Ti_{1.16}Nb_{2.63}O_{12}$+C+$C_3N$
29	0.00	87.50	12.50	T_2N_5+N
30	96.00	4.00	0.00	C+C_3N
31	96.00	0.00	4.00	C+R
32	4.00	0.00	96.00	R+C
33	50.00	10.00	40.00	R+C+$Cu_{3.21}Ti_{1.16}Nb_{2.63}O_{12}$
34	57.78	17.78	24.44	$Cu_{3.21}Ti_{1.16}Nb_{2.63}O_{12}$+C3N+CN
35	59.46	14.41	26.13	$Cu_{3.21}Ti_{1.16}Nb_{2.63}O_{12}$+C3N+CN
36	0.00	4.00	96.00	R+TN
37	4.00	96.00	0.00	N+CN
38	53.49	46.51	0.00	CN+C_3N
39	45.95	54.05	0.00	CN+N
40	56.46	23.13	20.40	$Cu_{3.21}Ti_{1.16}Nb_{2.63}O_{12}$
41	31.00	31.00	38.00	R+CN
42	32.00	32.00	36.00	R+CN
43	50.00	5.00	45.00	C+R

[a] R: rutile solid solution; C: CuO; CN: $CuNb_2O_6$; T_2N_5: $Ti_2Nb_{10}O_{29}$; TN: $TiNb_2O_7$; C_3N: $Cu_3Nb_2O_8$.

the Cu-containing component of the phase diagram, Fig. 6, is represented as CuO_x to allow for variable valence state of Cu.

A limited range of Nb-doped TiO_2 rutile solid solutions was previously suggested [17], with a maximum extent of ca. 10–15 mol% Nb_2O_5 at 1445–1475 °C. This phase diagram study shows the extent of solid solutions decreases with decreasing temperature. In the current study, the limit was found to be less than 4 mol% Nb_2O_5 at 935 °C. Little evidence was found here for Ti solubility in Nb_2O_5 at 935 °C; again, literature reports [17] show a very limited range of solid solutions (up to 5 mol% TiO_2) at higher temperatures.

The remainder of the phase diagram is divided into several two- and three-phase compatibility regions. Two previously-reported binary phases (Nb_6TiO_{17} [23], $Nb_{24}TiO_{62}$ [24,25]) were not found in any of the specimens prepared here at 935 °C, but may perhaps form, with a lower limit of stability, at higher temperatures.

3.4. Electrical properties of $Cu_{3.21}Ti_{1.16}Nb_{2.63}O_{12}$

Low temperature impedance measurements were carried out to establish the magnitude and temperature dependence of the bulk relative permittivity, ε_r, and conductivity of CTNO. A RT impedance data set is shown in Fig. 7(a), to which CCTO data from

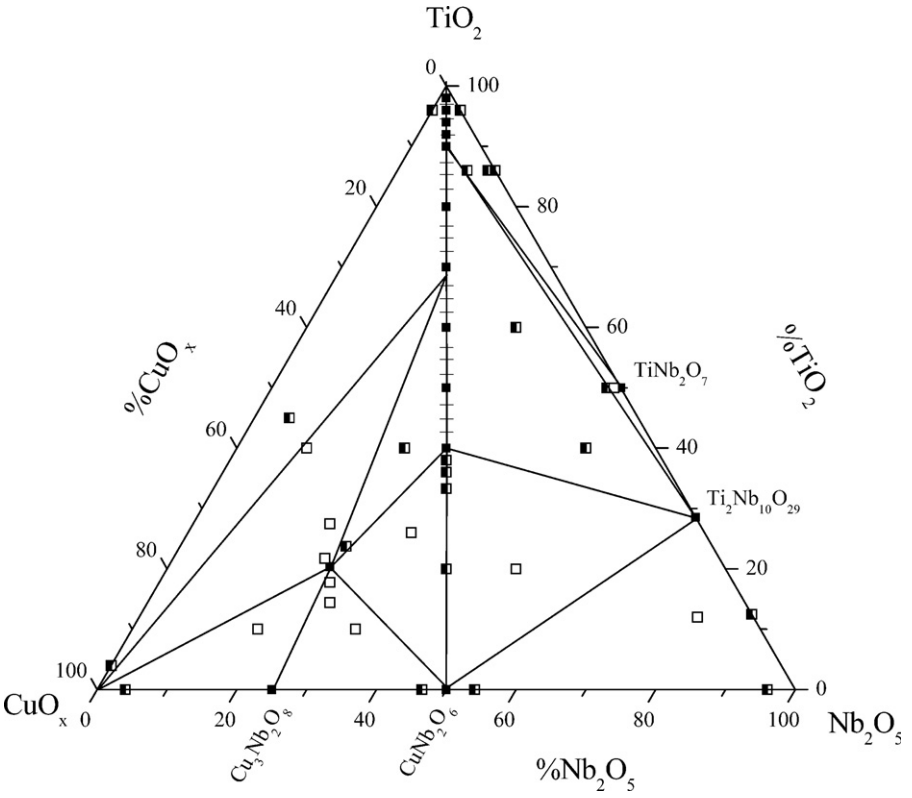

Fig. 6. Subsolidus phase relations at 935 °C for the CuO_x–TiO_2–Nb_2O_5 pseudoternary system. Closed (■), half closed (◧) and open squares (□) refer, respectively, to 1-, 2- and 3-phase products.

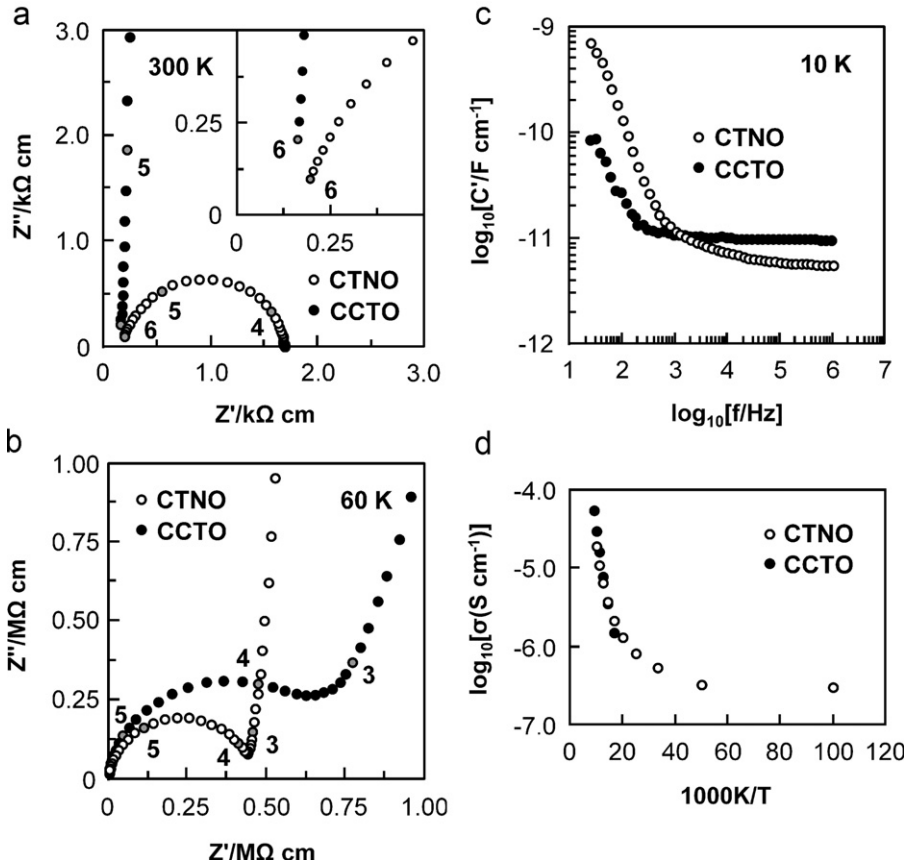

Fig. 7. Z^* plots of CTNO and CCTO at (a) RT and (b) 60 K. Selected log values of frequency are shown as gray circles. (c) C' spectroscopic plot of CTNO and CCTO at 10 K. (d) Arrhenius plot of CTNO and CCTO bulk conductivity.

Ref. [2] is added. CTNO exhibits a heterogeneous electrical microstructure similar to CCTO. A low frequency arc corresponding to the electrical response of the grain boundaries dominates the Z^* plot. A high frequency non-zero intercept is observed, shown clearly in the inset, which is caused by the bulk response at higher frequency. The almost identical non-zero intercept values for CTNO and CCTO demonstrates the bulk conductivity is similar at RT. At lower temperature, Fig. 7(b), the bulk arc is clearly visible. Impedance data obtained at 10 K are replotted as capacitance C' vs frequency in Fig. 7(c) from which bulk ε_r was calculated from the limiting high frequency plateau value of the capacitance. Over the temperature range 10–100 K, where the bulk response was readily accessed by impedance measurements, ε_r is $\sim$63 and displays very little temperature dependence. An Arrhenius plot of bulk conductivity ($\sigma = 1/R$) for CTNO and CCTO is shown in Fig. 7(d). Both display non-Arrhenius-type behavior, especially CTNO at low temperatures, and have a similar magnitude of conductivity above $\sim$50 K. These results indicate the conduction mechanism in CTNO is similar to that of CCTO.

A Clausius-Mossotti calculation based on ion polarisabilities and cell volume estimates ε_r of CTNO to be $\sim$27. The experimental value is considerably higher ($\varepsilon_r \sim 60$) and similar trends are observed for other members of this family, *e.g.*, CCTO ε_r (calculated) $\sim$48 and ε_r (observed) $\sim$100 and $Na_{1/2}Bi_{1/2}Cu_3Ti_4O_{12}$ (NBCTO) ε_r (calculated) $\sim$57 and ε_r (observed) $\sim$250 [26]. Although the origin(s) of this additional polarization has not been identified, we have recently shown CCTO and NBCTO to be incipient ferroelectrics [27,28] that display increasing ε_r with decreasing temperature. CTNO differs from CCTO and NBCTO in that ε_r does not display a strong temperature dependence suggesting that the presence of *A*-site cation(s) plays an important role in both the magnitude and temperature dependence of the ε_r in this family of materials.

4. Conclusions

The subsolidus phase relations in the CuO_x–TiO_2–Nb_2O_5 pseudo-ternary system were determined following heat treatments on 43 compositions. The phase diagram contains one new phase, $Cu_{3.21}Ti_{1.16}Nb_{2.63}O_{12}$, and one solid solution series, $Ti_{1-3x}Cu_xNb_{2x}O_2$: $0 < x < 0.2335 \pm 0.0035$ at 935 °C. The remainder of the phase diagram is divided into several two- and three-phase compatibility regions. Two previously-reported binary phases (Nb_6TiO_{17}, $Nb_{24}TiO_{62}$) were not found in any of the specimens prepared here at 935 °C. CTNO has similar electrical properties to CCTO, but with a bulk, temperature-independent permittivity of 63.

Acknowledgment

We thank EPSRC for funding.

References

[1] D.C. Sinclair, T.B. Adams, F.D. Morrison, A.R. West, Appl. Phys. Lett. 80 (12) (2002) 2153–2155.
[2] M.C. Ferrarelli, D.C. Sinclair, A.R. West, H.A. Dabkowska, A. Dabkowski, G.M. Luke, J. Mater. Chem. 19 (33) (2009) 5916–5919.
[3] M. Labeau, B. Bochu, J.C. Joubert, J. Chenavas, J. Solid State Chem. 33 (2) (1980) 257–261.
[4] Z. Zeng, M. Greenblatt, M.A. Subramanian, M. Croft, Phys. Rev. Lett. 82 (1999) 3164.
[5] A.M. Glazer, Acta Cryst. B28 (11) (1972) 3384–3392.
[6] M. O'Keeffe, B.G. Hyde, Acta Cryst. B33 (12) (1977) 3802–3813.
[7] A. Collomb, D. Samaras, B. Bochu, J.C. Joubert, Phys. Stat. Sol. A 41 (2) (1977) 459–463.
[8] J. Chenavas, J.C. Joubert, M. Marezio, B. Bochu, J. Solid State Chem. 14 (1) (1975) 25–32.
[9] A. Collomb, D. Samaras, J.L. Buevoz, J.P. Levy, J.C. Joubert, J. Magn. Magn. Mater. 40 (1-2) (1983) 75–82.
[10] M.A. Subramanian, D. Li, N. Duan, B.A. Reisner, A.W. Sleight, J. Solid State Chem. 151 (2) (2000) 323–325.
[11] A.P. Ramirez, M.A. Subramanian, M. Gardel, G. Blumberg, D. Li, T. Vogt, S.M. Shapiro, Solid State Commun. 115 (5) (2000) 217–220.
[12] M. Li, A. Feteira, D.C. Sinclair, A.R. West, Z. Shen, M. Nygren, J. Appl. Phys. 106 (2009) 104106.
[13] T.B. Adams, D.C. Sinclair, A.R. West, J. Am. Ceram. Soc. 89 (10) (2006) 3129–3135.
[14] B.H. Toby, J. Appl. Crystallogr. 34 (2001) 210–213.
[15] A.C. Larson, R.B. Von Dreele, General structure analysis system (GSAS), Los Alamos National Laboratory Report LAUR, 2000, pp. 86–748.
[16] Scribner Associates Inc., Z view for windows: impedance/gain phase graphing and analysis software, Southern Pines, North Carolina, 2001.
[17] T.G. Babich, A.V. Zagorodnyuk, G.A. Teterin, M. Ya., Khodos, A.P. Zhirnova, Zh. Neorg. Khim. 33 (4) (1988) 996–999;
T.G. Babich, A.V. Zagorodnyuk, G.A. Teterin, M. Ya., Khodos, A.P. Zhirnova, Russ. J. Inorg. Chem. (Engl. Transl.) 33 (4) (1988) 560–563.
[18] R.C. Pullar, J. Am. Ceram. Soc. 92 (3) (2009) 563–577.
[19] R.D. Shannon, Acta Cryst. A32 (1976) 751–767.
[20] PDF Card 46-524, JCPDS—Joint Committee of Powder Diffraction Standards, International Centre for Diffraction Data, USA, 2004.
[21] M.A. Subramanian, A.W. Sleight, Sol. State Sci. 4 (3) (2002) 347–351.
[22] B. Rivas-Murias, M. Sanchez-Andujar, J. Rivas, M.A. Senaris-Rodriguez, Mater. Chem. Phys. 120 (2–3) (2010) 576–581.
[23] R.S. Roth, L.W. Coughanour, J. Res. Natl. Bur. Stand. (U.S.) 55 (4) (1955) 209–213.
[24] N.F. Fedorov, O.V. Mel'nikova, V.A. Saltykova, A.P. Pivovarova, M. Dib, V.I. Strakhov, Zh. Neorg. Khim. 34 (5) (1989) 1316–1319;
N.F. Fedorov, O.V. Mel'nikova, V.A. Saltykova, A.P. Pivovarova, M. Dib, V.I. Strakhov, Russ. J. Inorg. Chem. (Engl. Transl.) 34 (5) (1989) 741–744.
[25] R.S. Roth, Prog. Solid State Chem. 13 (2) (1980) 159–192.
[26] M.C. Ferrarelli, T.B. Adams, A. Feteira, D.C. Sinclair, A.R. West, Appl. Phys. Lett. 89 (2006) 212904.
[27] M. Li, A. Feteira, D.C. Sinclair, A.R. West, Appl. Phys. Lett. 91 (2007) 132911.
[28] M.C. Ferrarelli, D. Nuzhnyy, D.C. Sinclair, S. Kamba, Phys. Rev. B 81 (2010) 224112.